Journal of King Saud University - Science 36 (2024) 103432

HOSTED BY

Contents lists available at ScienceDirect

Journal of King Saud University - Science

journal homepage: www.sciencedirect.com

Characterization and toxicity evaluation of chitosan/ZnO nanocompoite as promising nano-biopolymer for treatment of synthetic wastewater

Syeda Khola Tazeen [a], Muhammad Bilal Khan Niazi [b], Manal Abdulaziz Binobead [c], Temoor Ahmed [d,e], Muhammad Shahid [a,*]

[a] Department of Bioinformatics & Biotechnology, Government College University Faisalabad 38000, Pakistan
[b] Department of Chemical Engineering, School of Chemical and Materials Engineering, National University of Sciences and Technology, Islamabad 44000, Pakistan
[c] Department of Food Science and Nutrition, College of Agriculture Food Science, King Saud University, Riyadh, Saudi Arabia
[d] Xianghu Laboratory, Hangzhou 311231, China
[e] State Key Laboratory of Rice Biology and Breeding, Ministry of Agriculture Key Laboratory of Molecular Biology of Crop Pathogens and Insects, Key Laboratory of Biology of Crop Pathogens and Insects of Zhejiang Province, Institute of Biotechnology, Zhejiang University, Hangzhou, China

ARTICLE INFO

Keywords:
Textile wastewater
Chitosan/ZnO nanocomposite
Photocatalyst
Reactive black 5 dye
Phytotoxicity
Cytotoxicity

ABSTRACT

Nanotechnology advances wastewater treatment through the application of Nano entities that optimize contaminant removal and enhance water purification efficacy. In this study, ZnO nanoparticles (ZnO NPs) were synthesized using *Klebsiella pneumoniae*, subsequently, a chitosan/ZnO nanocomposite (CS/ZnO NC) was prepared for removing reactive black 5 (RB-5) dye from synthetic wastewater. The biosynthesized nanomaterials were characterized using UV–VIS, FTIR, XRD, SEM and TEM techniques. The UV–Vis absorbance peaks at 370 nm and 350 nm corresponded to the characteristic surface plasmon resonance of ZnO NPs and the CS/ZnO NC, respectively. Additionally, FTIR analysis identified the various functional groups associated with ZnO NPs and the CS/ZnO NC. XRD analysis revealed their crystallinity to be approximately 22.44 and 25.76, respectively. The SEM images of ZnO NPs and the CS/ZnO NC show hexagonal plate-like particles with sizes of 33.66 nm and 38.64 nm, respectively. Four concentrations of ZnO NPs and CS/ZnO NC (0.25, 0.5, 1, and 2 mg/mL) were evaluated for RB-5 degradation at three different levels (25, 50, and 100 mg/L). Statistical analysis showed that chitosan/ZnO NC achieved 95 % dye degradation, compared to 81 % degradation with the same amount of ZnO nanoparticles. Furthermore, a pot experiment was carried out to evaluate the phytotoxicity effects of treated wastewater on wheat (*Triticum aestivum L.*). Both ZnO NPs and CS/ZnO NC did not significantly affect the viability of epithelial retinal cell lines at concentrations up to 100 μg/mL, suggesting a safe cytotoxic profile within this dosage range. Overall, CS/ZnO NC proved effective for treating industrial wastewater, making it suitable for recycling in agricultural applications

1. Introduction

Despite the fact that water is the vital element for the survival of human life on earth, it is facing prodigious challenges. The pharmaceutical, textile, paper, plastic and cosmetics industries produce more than 100,000 tons of dyes each year and about 8–20 % of these dyes drained out directly into water reservoirs without treatment adversely affecting quality of the whole aquatic ecosystem (Castillo-Suarez et al., 2023). Moreover, such wastewater, when applied to agricultural soils due to the non-availability and unsuitability of underground water for agricultural purposes, especially in developing countries, not only disturbs the soil structure and health but also damages soil microbial balance (González-Fragozo et al., 2020). The prevalent physicochemical methods for removing textile dyes from wastewater include precipitation, photocatalysis, adsorption, and advanced oxidation. Metallic oxide nanoparticles, such as iron oxide (Fe_2O_3), titanium dioxide (TiO_2), and zinc oxide (ZnO), have been identified as effective photocatalytic and adsorptive agents for wastewater treatment. Nanoparticles, particularly zinc oxide (ZnO), combined with the low-cost natural polymer chitosan, demonstrate promising potential as photocatalytic and adsorptive agents for wastewater recycling (Mutukwa et al., 2022). Singh et al. (2023) Revealed that ZnO graphene oxide nanocomposites also have

* Corresponding author.
E-mail address: mshahid@gcuf.edu.pk (M. Shahid).

https://doi.org/10.1016/j.jksus.2024.103432
Received 1 July 2024; Received in revised form 2 September 2024; Accepted 3 September 2024
Available online 4 September 2024

TiO_2 NPs like properties which completely mineralize azo dyes into H_2O, CO^2 and other nontoxic compounds. Recently, Hassaan et al. (2019) concluded that more than 80 % reactive black-5 (RB-5) dye decolorization occur when 3 mg/L ZnO NPs immobilized with ceramic surface are used under strong alkaline conditions. However, limited studies are available deciphering the comparative effect of nanoparticles and their polymer-based composites for degradation of azo dyes (Maruthupandy et al., 2020, Adeel et al., 2021, Maliki et al., 2022). This study employed green synthesis methods to produce ZnO nanoparticles and develop a CS/ZnO nanocomposite, evaluating their effectiveness in removing RB-5 dye from synthetic water through photocatalytic and adsorptive mechanisms. Additionally, it explored the agricultural reuse of dye-treated wastewater and assessed its cytotoxicity. The ultimate goal of this research is to advance nano-based textile wastewater treatment processes and facilitate their scaling up to pilot and industrial levels.

2. Materials and methods

2.1. Collection of bacterial strain

To synthesize biogenic ZnO NPs bacterial strain *Klebsiella pneumoniae* NST2 (Accession # MN121582) was obtained from cultural collection of Department of Bioinformatics and Biotechnology, Government College University Faisalabad (GCUF), Pakistan. The strain was originally isolated from the agricultural land adjacent to Paharang drain (N∘ 31 25′ 13 and E 73∘ 4′ 35), Faisalabad, Pakistan by our laboratory group and has already been employed to synthesize copper and silver NPs (Noman et al., 2021).

2.2. Extracellular green synthesis of ZnO NPs

ZnO NPs were synthesized using a previously established protocol with minor modifications. Bacterial cultures were cultivated in 250 mL Erlenmeyer flasks containing 100 mL of nutrient broth, continuously stirred at 28 ± 2 °C for 24 h. After incubation, the cultures were centrifuged at 6,000 g for 10 min to collect the supernatant. To this supernatant, 2 mM of zinc sulfate heptahydrate [$ZnSO_4{\cdot}7H_2O$; Sigma Aldrich, USA] was added as the precursor. The appearance of a white precipitate and a color shift from pale yellow to milky white, indicative of the reduction of Zn^{2+} ions, signaled the formation of ZnO NPs. The precipitates were then collected by centrifugation at 6,000 g for 15 min. The resulting pellet was washed twice with distilled water and 70 % ethanol to eliminate impurities, followed by freeze-drying at −60 °C. Finally, the pellet was ground into a fine powder and stored for subsequent analysis.

2.3. Synthesis of Chitosan/ZnO NC

The CS/ZnO NC was prepared by mixing 1 g of ZnO NPs into a 99 % (w/v) chitosan solution and stirring for 15 min. The pH was adjusted to 10 with 1 M NaOH, and the solution was stirred for 3 h before being heated at 60 °C for 1 h in a water bath. The nanocomposites were then filtered, washed with distilled water, freeze-dried at −60 °C for 4 h, and stored for future use.

2.4. Characterization of biogenic ZnO NPs and CS/ZnO NC

The characteristics of ZnO NPs and CS/ZnO NC were analyzed using several methods. UV–Vis spectroscopy (Schimadzu UV/VIS, Japan) measured absorbance in the 200–800 nm range. Scanning electron microscopy (SEM) (Hitachi TM-1000, Japan) assessed particle size and surface morphology. Fourier transform infrared (FT-IR) spectroscopy (Perkin Elmer Spectrum BX) analyzed functional groups from 4000 to 400 cm^{-1}. X-ray diffraction (XRD) (Thermo Scientific K-Alpha, USA) was used to study crystallographic structure and phase transitions.

2.5. Degradation of RB-5 dye

For dye degradation studies, 0.5 g of RB-5 dye was dissolved in 100 mL of distilled water to prepare a 5000 mg/L stock solution. Various working solutions (25, 50, 100 mg/L) were then treated with different concentrations (0.25, 0.5, 1, and 2 mg/mL) of ZnO NPs, CS/ZnO NC, CS, and $ZnSO_4$. The treatments were exposed to sunlight and kept in the dark for 5 h each to assess photocatalytic and adsorption efficiency. Samples were collected at 1, 2, 3, 4, and 5 h, and dye degradation was measured using a UV–Vis spectrophotometer (U-5100, Hitachi) at λmax = 595 nm. The amount of photocatalytic degradation/adsorption were calculated according to the following formula.

$$\text{Decolorization}\,(\%) = \frac{(A - B)}{A} \times 100$$

Where A and B represent the initial and final absorbance of the dye solutions.

To evaluate the impact of pH on the photocatalytic and absorptive removal of RB-5 dye, experiments were conducted using an optimized dye concentration of 50 mg/L and catalyst concentration of 0.5 mg/mL. pH levels ranged from 3 to 10, and dye removal was assessed using the previously described spectrophotometric method.

2.6. Phytotoxicity evaluation of nanomaterials

To assess the environmental risk of nanomaterials, a plant experiment was conducted to examine the effects of photo catalyzed (treated) and non-treated RB-5 dye solutions on wheat growth and physiological parameters. The study used RB-5 dye degraded by various concentrations (0.25, 0.5, 1, and 2 mg/mL) of ZnO NPs and CS/ZnO NC, with distilled water as a control. Twenty seeds per treatment were placed in petri dishes (three replicates each) and incubated for 25 days at 25°C with a 16-hour light/8-hour dark cycle and 70 % humidity. Growth parameters, including root length (RL), shoot length (SL), fresh and dry weights, as well as antioxidant and oxidant levels, were measured. H_2O_2 content was estimated using a method involving leaf extract and titanium sulfate, and peroxidase (POD), catalase (CAT), and ascorbate peroxidase (APX) activities were measured spectrophotometrically.

2.7. Cytotoxicity evaluation of nanomaterials

To assess cytotoxicity, ZnO NPs and CS/ZnO NC were tested on a retinal pigment epithelium (RPE) cell line using the MTT assay. RPE cells were seeded at 2×10^5 cells per well in 96-well plates and incubated for 24 h in Dulbecco's Modified Eagle (DME) Medium. They were then exposed to various concentrations (0, 25, 50, 100, and 200 μg/mL) of NPs and NC for 24 h. Phosphate-buffered saline (PBS) served as the positive control. After 3 days, MTT solution (5 mg/mL) was added, and absorbance was measured at 570 nm.

2.8. Statistical analysis

Data for RB-5 degradation and phytotoxicity were analyzed using Statistix v 8.1. Three-way analysis of variance (ANOVA) was used for multiple comparison followed by correction using LSD analysis. Obtained valves were statistically significant at $P < 0.05$.

3. Results

3.1. Biogenic synthesis of ZnO NPs and CS/ZnO NC

Results on the synthesis of ZnO NPs indicated that the capping agents coming from the strain *Klebsiella pneumoniae* NST2 were able maximize the synthesis of ZnO NPs at 2 mM concentration of $ZnSO_4$ salt. Out of the many precursor salt concentrations (1, 2, 3, 4 and 5 mM) tested, 2 mM

was used for the biogenic synthesis of ZnO NPs. The formation of white precipitates at the bottom of flask was the first morphological indication of ZnO NPs synthesis shown in Fig. 1 (b). Then these ZnO NPs were used for the production of CS/ZnO NC using the methods reported earlier by some researchers (Sabrin and Arafat 2015, Bashal et al., 2022, Zaman et al., 2022). Prepared ZnO NPs was further mixed with CS to form CS/ZnO NC. The formation of white precipitate was primary indication of CS/ZnO NC formation (Preethi et al., 2020). Initially, to confirm the formation of ZnO NPs, the nano material was characterized by the UV–vis absorption spectrum. A sharp adsorption edge was observed at 370 nm confirmed the ZnO NPs synthesis. For CS/ZnO NC blue shift of the adsorption band to 350 nm was observed which is in a characteristic peak range for CS/ZnO NC (Fig. S1).

3.2. FT-IR analysis

FT-IR measurement spectrum illustrated molecular structure, chemical bond and elemental composition of ZnO NPs and CS/ZnO NC. In this technique, functional groups present in a molecule absorbed a certain range of frequency transmission of infrared (IR) radiation resulted in stretching and bending of various molecular bonds. The FT-IR spectra of ZnO NPs and CS/ZnO NC are presented in Fig. 1A ZnO nano powder showed peak at 3413 cm^{-1} which depicted O–H stretching vibration of chemosorbed water. Frequency bands of the FT-IR spectrum present at 2956–2926 cm^{-1} attributed to the C–H bond stretching vibration. Further, the sharp peak at 1652 cm^{-1} indicated medium C=C stretching. The peak at 1538 cm^{-1} was due to the strong stretching vibration of N-O nitro compounds. Moreover, the C–H medium bending was due to the presence of FT-IR spectrum peak at 1449 cm^{-1}. Characteristic peaks at 1413 cm^{-1}, 1236 cm^{-1} and 1082 cm^{-1} indicated the S=O, C-O and C-O stretching vibration respectively. The band spectrum in the range of 528–435 cm^{-1} denoted representative stretching mode of Zn-O. Similarly, Fig. 1A also depicted the –OH/–NH_2 bond stretching vibration at 3409 cm^{-1}.The FT-IR spectrum peaks at 2921 and 2201 cm^{-1} were referred to the C–H and C≡C stretching vibration. Compared to the spectrum of ZnO, an additional band from 577 to 420 cm^{-1} attributed to the Zn-O stretching vibration, which appears in the spectrum of the CS/ZnO NC. This stretching referred to the presence of ZnO in the structure of the composite. Moreover, the –OH/–NH_2 stretching vibration at 3413 cm^{-1} moved to the lower wavenumber (3409 cm^{-1}) in the composite, signifying the strong inter-molecular hydrogen bond interaction between ZnO and CS. The CS/ZnO composite benefits from chitosan (CS), adding more amino (NH_2) groups to the material. Chitosan, a polysaccharide comprising glucosamine units, features amino groups (–NH_2) along its polymer backbone. Consequently, the absorption peak at 3423 cm^{-1} in the CS-ZnO composite likely results from the stretching vibration of hydroxyl (–OH) groups from ZnO and amino (–NH_2) groups from chitosan.

3.3. XRD analysis

The XRD spectrum peaks of ZnO NPs and CS/ZnO NC are shown in Fig. 1B ZnO NPs depicted strong broad diffraction peaks at 31.7 (cm^{-1}), 34.35 (cm^{-1}), 36.2 (cm^{-1}), 47.53(cm^{-1}), 56.15(cm^{-1}) and 62.5(cm^{-1}) which were equivalent to the structure of the JCPDS: 36-1451 of ZnO. Furthermore, the XRD peaks pattern illustrated strong peaks matching to the ZnO diffraction pattern. However, the peaks pattern of CS/ZnO NC was similar to ZnO NPs but the intensity of peaks at some points are lower indicating interference between ZnO and CS functionalities. Moreover, some changes related with peaks positions and length signifying the adjustments of ZnO NPs due to the composite fabrication. Table 1 shows the crystallite size of ZnO NPs and CS/ZnO NC estimated by Scherrer's equation.

3.4. SEM analysis

The SEM image of pure ZnO NPs and CS/ZnO NC nano powder displayed external shape of the NPs with morphology and surface (Table 1).

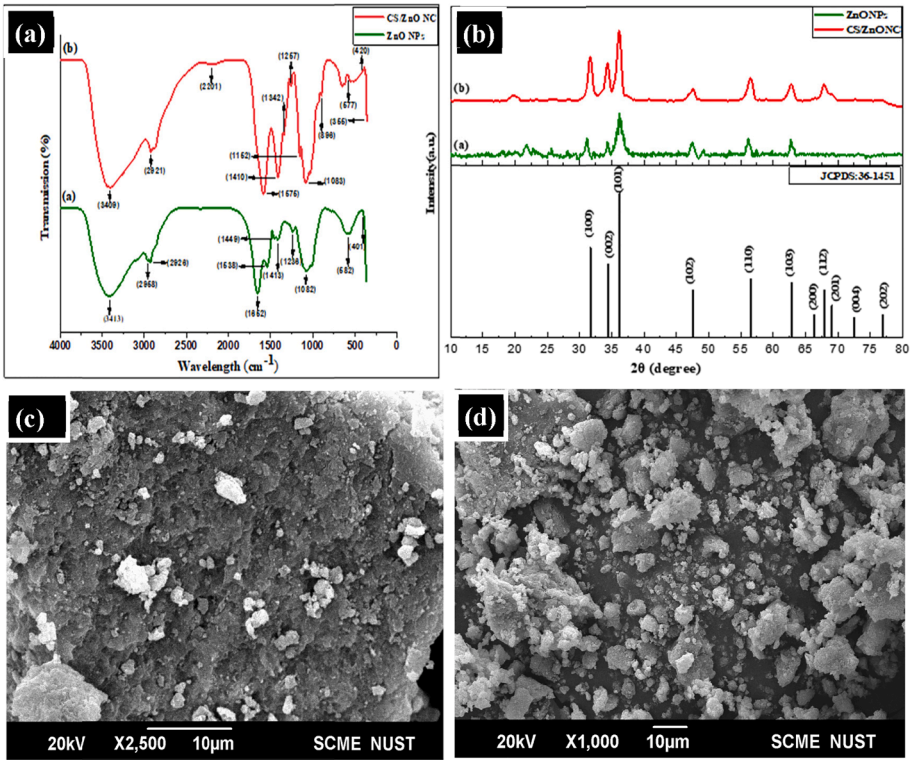

Fig. 1. (a) FT-IR band spectrum of synthesized nanomaterials **(b)** XRD crystallographic analysis of biologically synthesized ZnO nanoparticles and CS/ZnO nanocomposite **(c)** SEM image of ZnO NPs at 2.5KX magnification **(d)** SEM image of CS/ZnO NC at 2.5KX magnification.

Table 1
The size and specific surface area of ZnO NPs and CS/ZnO NC.

Nano sample	Scanning electron microscopy (SEM)	X-ray diffraction (XRD)	Shape
ZnO NPs	33.66 nm	22.44	Hexagonal plates
CS/ZnO NC	38.64 nm	25.76	Spherical

The morphology of the particles increases the surface area with more chances of metal adsorption shown in Fig. 1C & D.

3.5. Effect of dye concentration on photocatalytic and adsorptive removal of RB-5

Three different concentrations (25, 50 and 100 mg/L) of RB-5 were decolorized by different catalysts (ZnO NPs, CS/ZnO NC, CS and $ZnSO_4$) for 5 h. The efficiency of dye degradation significantly decreases by increasing dye concentration. At 25 mg/L dye concentration and 2 mg/mL catalyst concentration photocatalytic degradation of RB-5 was observed 81 %, 95 %, 51 % and 14 % for ZnO NPs, CS/ZnO NC, CS and

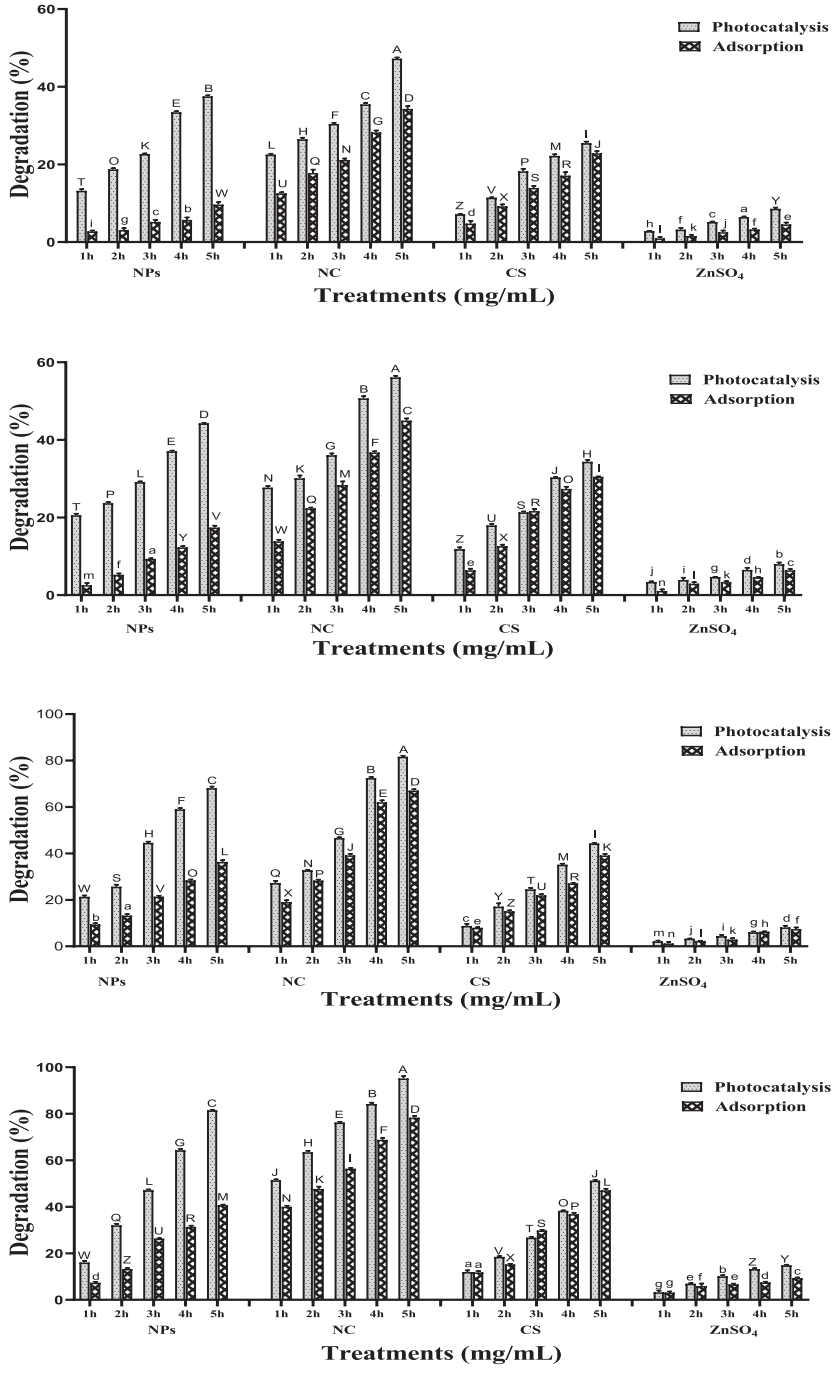

Fig. 2. Effect of different photocatalyst and adsorbent (ZnO nanoparticles, CS/ZnO nanocomposite, chitosan and $ZnSO_4$) on degradation of RB-5 at dye concentration of 25 mg/L using different Catalysts concentrations **(a)** 0.25 mg/mL **(b)** 0.5 mg/mL **(c)** 1 mg/mL **(d)** 2 mg/mL in both light and dark conditions for 5 h.

$ZnSO_4$ respectively which is significantly dissimilar from adsorptive degradation which was 40 %, 78 %, 47 % and 9 % for ZnO NPs, CS/ZnO NC, CS and $ZnSO_4$ respectively after 5 h shown in Fig. 2. At 50 mg/L dye concentration photocatalysis was recorded 72 %, 83 %, 45 % and 11 % for ZnO NPs, CS/ZnO NC, CS and $ZnSO_4$ respectively, which is significantly different from adsorptive degradation, which was 35 %, 66 %, 29 % and 6 % for ZnO NPs, CS/ZnO NC, CS and $ZnSO_4$ respectively after 5 h (Fig. 3). At 100 mg/L dye concentration photocatalysis was recorded 54 %, 71 %, 39 % and 8 % for ZnO NPs, CS/ZnO NC, CS and $ZnSO_4$ respectively which is differ from adsorptive degradation which was 27 %, 51 %, 20 % and 5 % for ZnO NPs, CS/ZnO NC, CS and $ZnSO_4$ respectively after 5 h shown in Fig. 4.

3.6. Effect of pH on photocatalytic and adsorptive removal of RB-5

Different pH levels were used to evaluate the highest RB-5 degradation efficiency using ZnO NPs, CS/ZnO NC, CS, and $ZnSO_4$ under both light and dark conditions. CS/ZnO NC showed significantly highest degradation 99 % and 98 % at 3 and 4 pH conditions as adsorptive and catalytic agent while ZnO NPs showed highest activity about 82 % as

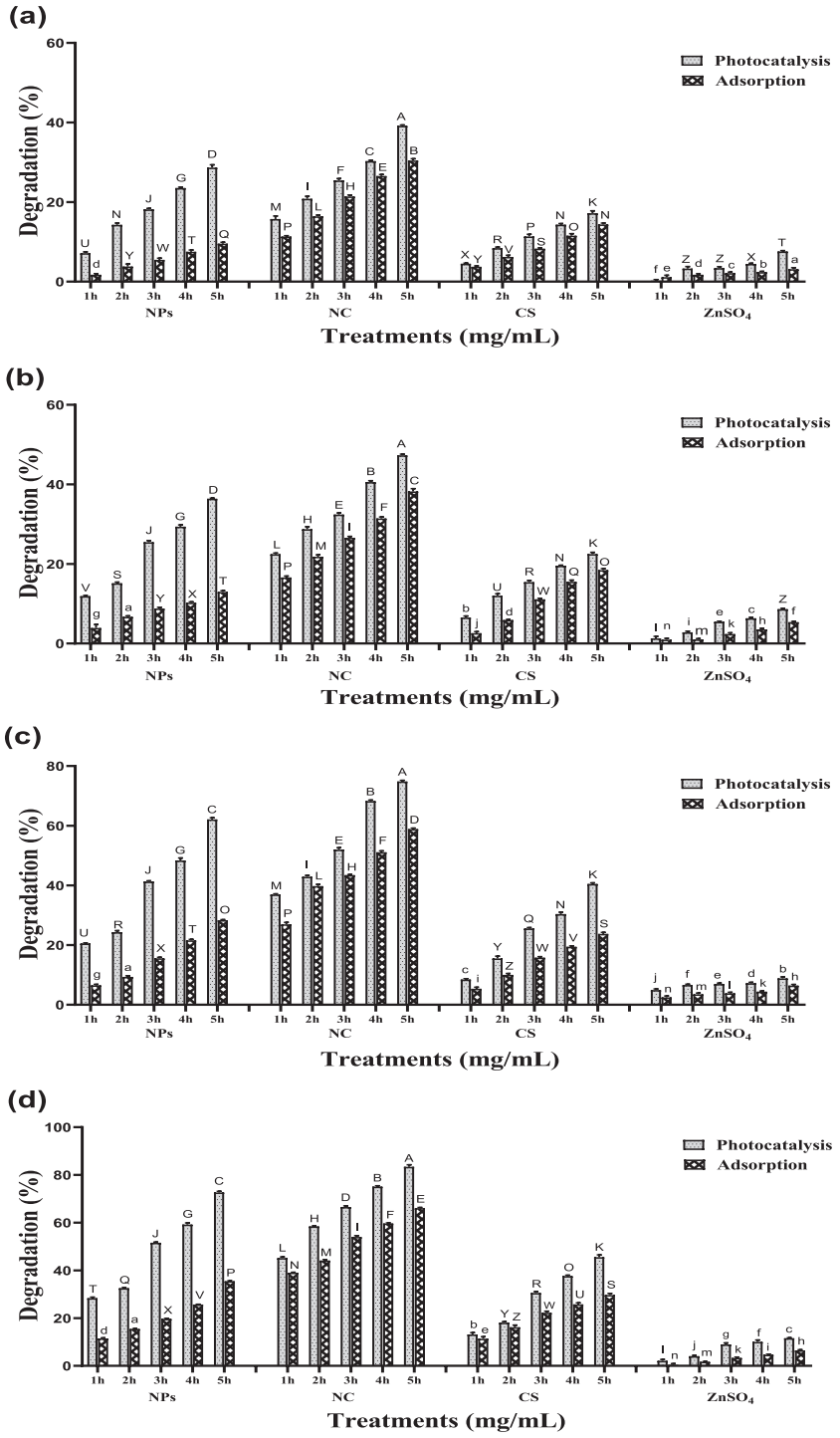

Fig. 3. Effect of different photocatalyst and adsorbent (ZnO nanoparticles, CS/ZnO nanocomposite, chitosan and $ZnSO_4$) on degradation of RB-5 at dye concentration of 50 mg/L using different Catalysts concentrations **(a)** 0.25 mg/mL **(b)** 0.5 mg/mL **(c)** 1 mg/mL **(d)** 2 mg/mL in both light and dark conditions for 5 h.

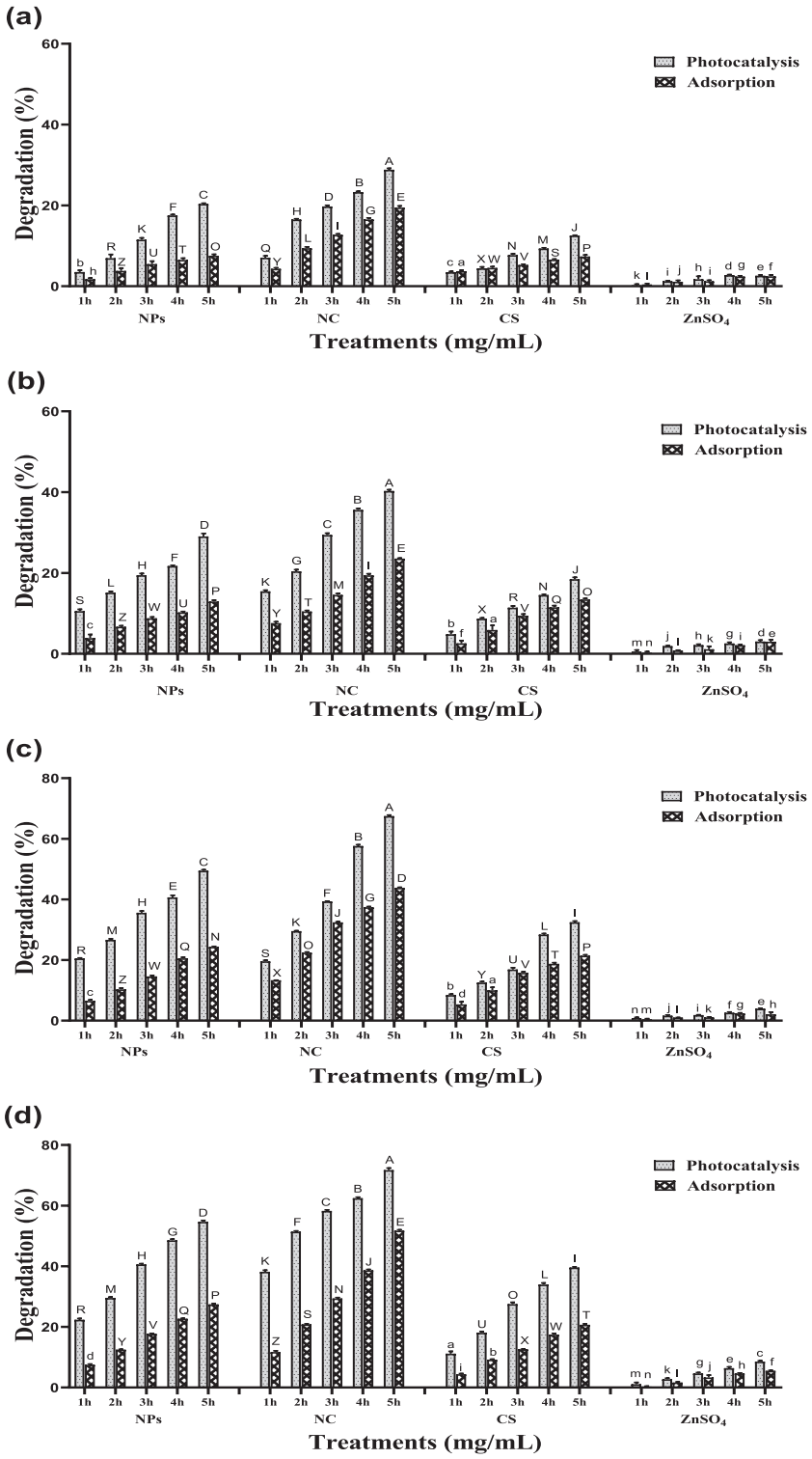

Fig. 4. Effect of different photocatalyst and adsorbent (ZnO nanoparticles, CS/ZnO nanocomposite, chitosan and $ZnSO_4$) on degradation of RB-5 at dye concentration of 100 mg/L using different Catalysts concentrations **(a)** 0.25 mg/mL **(b)** 0.5 mg/mL **(c)** 1 mg/mL **(d)** 2 mg/mL in both light and dark conditions for 5 h.

photocatalyst under acidic conditions (3 pH) shown in Fig. 5. However, CS degrade about 58 % RB-5 dye at 3 pH. $ZnSO_4$ showed maximum 12 % degradation at basic conditions.

3.7. Phytotoxicity experiment

3.7.1. Morphological parameters

In phytotoxicity studies, the SL of wheat plant treated with ZnO NPs at 1 mg/mL concentration was higher 18 % than control 16 % which was treated with distilled water (Fig. S2). RL was significantly high 16 % when treated with CS/ZnO NC and $ZnSO_4$ at 2 and 0.25 mg/mL

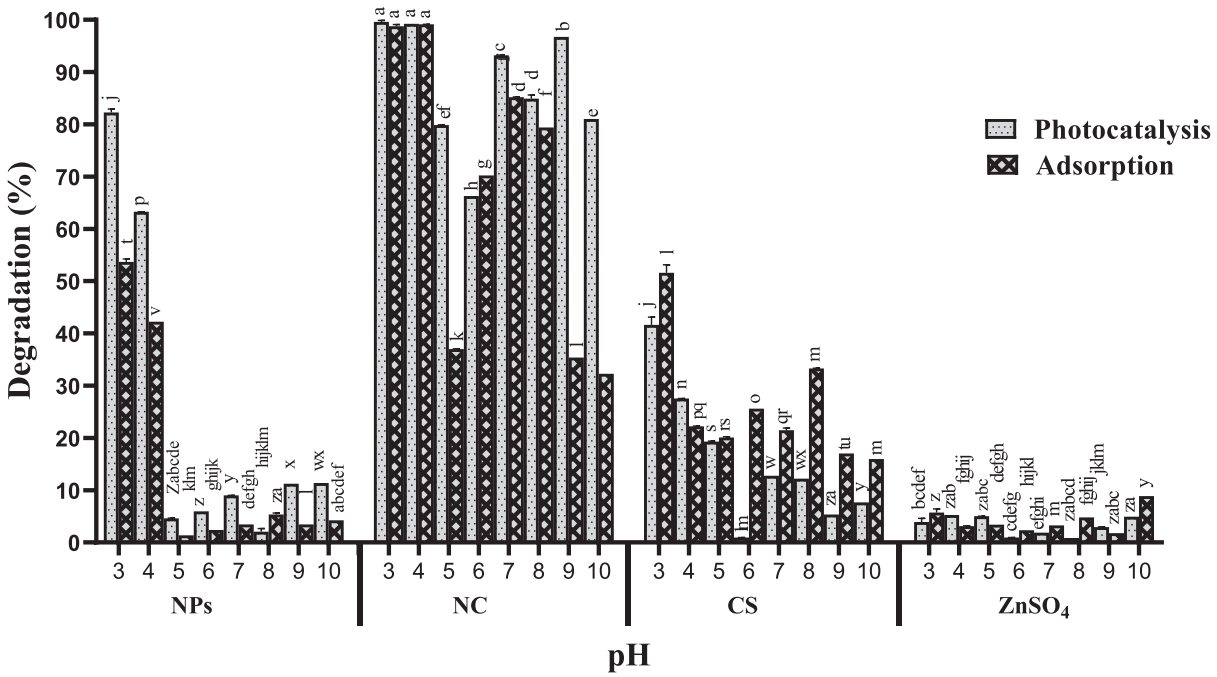

Fig. 5. Degradation of RB-5 at different pH levels (3–10), dye concentration (50 mg/L) using catalysts (ZnO nanoparticles, CS/ZnO nanocomposite, chitosan and $ZnSO_4$) on concentration (0.5 mg/mL) under both light and dark conditions for 5 h.

concentration. SDW and RDW was significantly high in the presence of CS/ZnO NC. In the phytotoxicity experiment, the SL of wheat plant was increased 11 %, 30 % and 15 % at 0.25, 0.5 and 1 mg/mL concentration of ZnO NPs respectively, but it decreased about 35 % at maximum 2 mg/mL concentration of ZnO NPs. While SL was increased 20 %, 36 %, 22 % at CS/ZnO NC concentration of 0.25, 0.5 and 1 respectively, but decrease 28 % at highest concentration. Similarly, RL was increase 7 %, 25 % and 20 % while treated with ZnO NPs and 11 %, 37 % and 26 % when CS/ZnO NC applied at 0.25, 0.5 and 1 mg/mL concentration respectively. Likewise, SFW and SDW was increase 17 %, 44 %, 28 % and 1 %, 33 %, 6 % at 0.25, 0.5 and 1 mg/mL ZnO NPs and 23 %,57 %, 30 % and 16 %, 39 %, 10 % at same CS/ZnO NC concentration respectively. While SFW and SDW decrease 27 % and 64 % for ZnO NPs and 22 %, 50 % for CS/ZnO NC at 2 mg/mL high concentration of nano catalyst respectively. Similarly, RFW and RDW was increase 30 %, 38 %, 33 % and 13 %, 29 %, 19 % with ZnO NPs. Plant showed same pattern of RFW and RDW increase of 35 %, 49 %,40 % and 24 %, 33 %,23 % when treated with CS/ZnO NC. Significant difference in growth of above growth parameters is shown in Fig. 6.

3.7.2. *Photosynthetic parameters*

CS/ZnO NC has increased the photosynthetic pigments such as Chlorophyll *a*, chlorophyll *b*, carotenoids and total chlorophyll by 46 %, 60 %, 62 % and 55 % respectively at 0.5 mg/mL concentration. ZnO NPs showed increase in values of Chlorophyll *a*, chlorophyll, carotenoids and total chlorophyll by 34 %,54 %, 57 % and 47 % respectively as the same concentration. After threshold value of 1 mg/mL photosynthetic pigments decreased as compared to control by 49 %,25 % 34 % and 55 % for ZnO NPs and 31 %,13 %,45 % and 6 % for CS/ZnO NC (Fig. 7).

3.7.3. *Antioxidant and oxidant enzymes*

Antioxidants such as POD, CAT and APX production were increase by applying CS/ZnO NC 42 %, 24 % and 46 % at 0.5 mg/mL as compared to control. At the same concentration (0.5 mg/mL) POD, CAT and APX production also increased 38 %, 18 % and 37 % in comparison to control. While ZnO NPs and CS/ZnO NC showed significant decrease in H_2O_2 production about 42 % and 33 % respectively shown in Fig. 7.

3.8. *Cytotoxicity assessment*

In MTT assay which was performed RPE cell lines, the cell viability graph showed up to 96 % and 98 % cell survival rate for ZnO NPs and CS/ZnO NC, respectively. However, the survival rate at 200 µg/mL percentage of cell viability was found statistically significant. Percentage of cell viability was observed about 53 % for ZnO NPs and 79 % for CS/ZnO NC at highest concentration of 200 µg/mL as shown in Fig. 8.

4. Discussion

In this study, ZnO NPs were biologically synthesized, offering an eco-friendly and cost-effective approach. During preparation ZnO NPs exhibited milky precipitation in aqueous solution, indicating effective reduction of Zn^{2+} ions to ZnO NPs after adding zinc sulfate to the culture filtrate. Additionally, Zn^{2+} ions interacted electrostatically with the –OH and $–NH_2$ groups of chitosan (CS) macromolecules, creating a nanoscale surface that facilitated nanoparticle growth in the CS/ZnO nanocomposite (Alzahrani et al., 2023). In addition, UV–Visible absorption spectra of ZnO NPs, CS/ZnO NC were clearly different in terms of λmax than pure CS and $ZnSO_4$. Chitosan and ZnO NPs may undergo a chemical reaction where in the amino groups ($–NH_2$) of chitosan coordinate with zinc ions (Zn^{2+}) on the ZnO surface, forming coordination bonds. This could result in the formation of a chitosan-ZnO complex, potentially stabilizing the nanoparticles and influencing the properties of the resulting Chitosan/ZnO nanocomposite (Kumar et al., 2021).

Moreover, the UV–vis spectrum of pure CS did serve as a control to distinguish it from CS/ZnO NC in UV–vis spectroscopy (Thamilarasan et al., 2018). Moreover, SEM imaged described shaped CS/ZnO NC embedded into porous matrix of chitosan (Zeghoud et al., 2022). Many studies shows that CS/ZnO nanocomposite have great efficiency to treat wastewater pollutant due to presence of charged functional groups (Bashal et al., 2022, Malekkiani et al., 2022, Zaman et al., 2022, Jyoti et al., 2023, Rahman et al., 2023). ZnO NPs are most effective for dye degradation due to its stability and semi conductive nature (Batra et al., 2022). On the other hand, when metal oxide combined with polymers such as chitosan, it also enhanced rate of separation of electron holes, which boosts photon irradiation, leading to increase photocatalytic

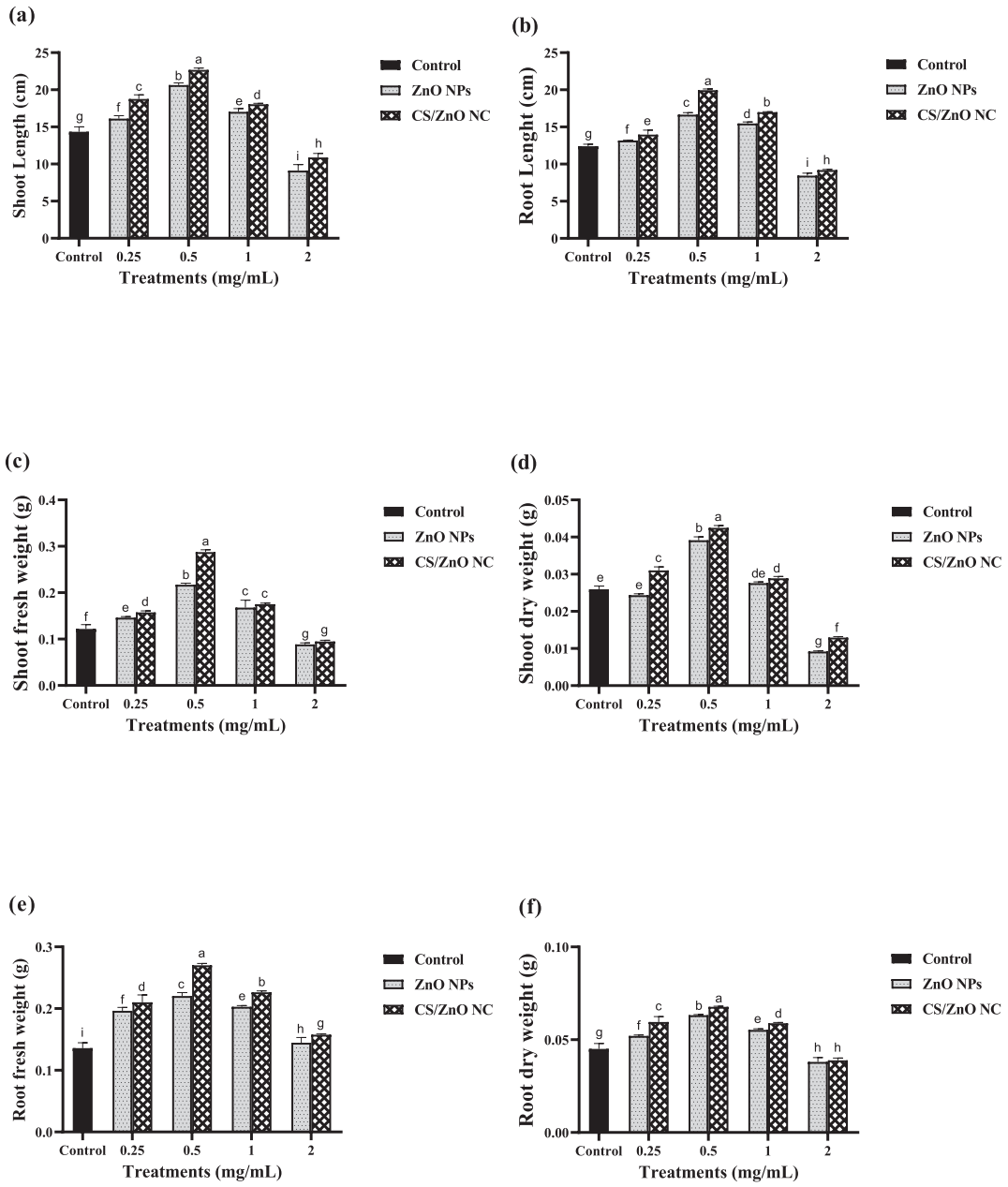

Fig. 6. Comparative effect of distilled water treated with ZnO NPs, CS/ZnO NC, CS and $ZnSO_4$ and non-treated water (control) **(a)** Shoot length **(b)** Root length **(c)** Shoot fresh weight **(d)** shoot dry weight **(e)** root fresh weight **(f)** root dry weight of wheat plants. Values are used in above graphs are means of triplicate and different letters represent the statistical significance ($P \leq 0.05$) among the treatment means.

activity (Malagutti et al., 2009, Díaz et al., 2022). The material characteristics of ZnO NPs and CS/ZnO NC were found much comparable with those reported by earlier researchers (Mekahlia and Douadi 2021, Alzahrani et al., 2023). For example, the XRD peaks pattern of ZnO NPs and CS/ZnO NC found in current study was similar to those reported earlier by (Ben Amor et al., 2022); however, some additional XRD peaks of ZnO NPs and CS/ZnO NC were also found in the current study which represented different diffraction angles of oxides of Zn and CS. Further, FTIR spectra confirmed cross linking of Zn with hydroxyl groups of CS biopolymer in CS/ZnO NC. Functional groups in FTIR spectra of ZnO NPs depicted the presence of reduced ZnO^{+} ions similar to the findings of (Bui et al., 2017). Moreover, SEM imaged described spherical shaped CS/ZnO NC embedded into porous matrix of chitosan. The presence of chitosan in the CS/ZnO NC are visible at 2913, 1676, 1342, 1083 cm^{-1} which are similar to previous studies (Kumar and Koh 2012, Chaisorn et al., 2023).

Although many reports are present on photocatalytic degradation of RB-5 dye using ZnO nanoparticles (Hassaan et al., 2019, Samsami et al., 2020, Picos-Corrales et al., 2023, Ali et al., 2024) but a few researchers investigated the comparative photocatalytic and adsorptive degradation of RB-5 dye by employing ZnO NPs and CS/ZnO NC. In photocatalytic degradation, when ZnO NPs were exposed to light in the presence of aqueous dye solutions, photoexcitation occurred and RB-5 dye adsorbed on the ZnO surface in close proximity resulting in the formation of photo generated valence band hole (h^{+}) and electrons bands (e^{-}) (Maeda 2011). This electron shifting produced highly reactive hydroxyl radicals (OH^{-}) from water, which oxides RB-5 dye molecules resulting in the breakdown down of its chemical structure. This ultimately transformed RB-5 dye into less colored or colorless metabolites. This degradation of dye depends upon various other factors such as dye concentration, pH,

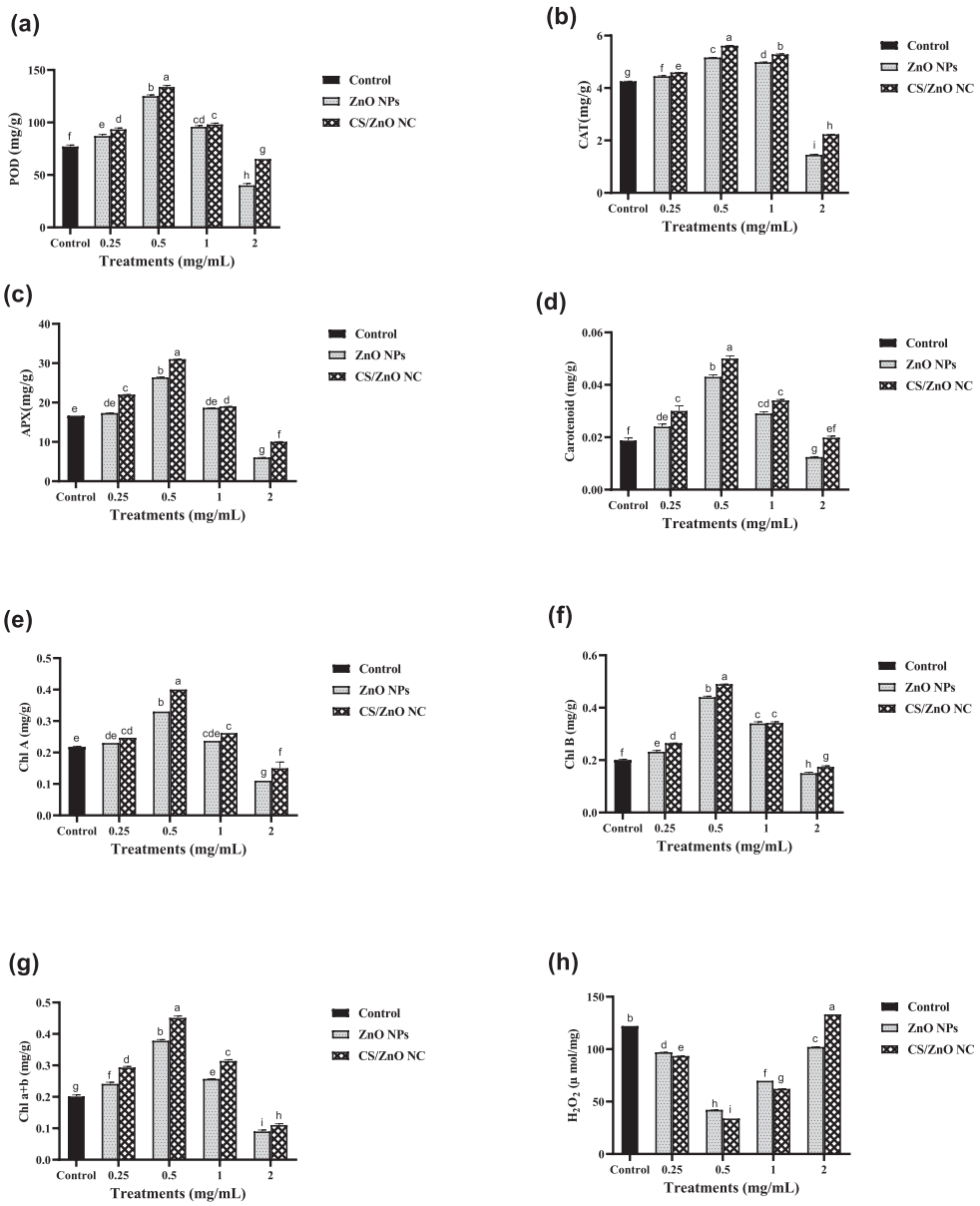

Fig. 7. Comparative effect of water treated with catalyst and non-treated water on different physiological parameters of wheat plant such as **(a)** POD **(b)** CAT **(c)** APX **(d)** carotenoids **(e)** chlorophyll *A* **(f)** chlorophyll *B* **(g)** total chlorophyll of wheat plants and **(h)** H_2O_2.Values used in above graphs are means of triplicate and different letters represent the statistical significance ($P \leq 0.05$) among the treatment means.

and reaction duration (Mathiarasu et al., 2021).

However, CS/ZnO NC can degrade RB-5 in both light and dark conditions due to presence of amino and hydroxyl group in CS (Kumar et al., 2021). These functional groups participate in redox reactions during photocatalysis and form a hydrogen bond with dye molecules which enhance adsorption of dye on CS surface (Shi et al., 2022). The significantly lower RB-5 degradation in dark condition occur when ZnO NPs were applied is due to less production of oxidative reactive species necessary for dye degradation due to absence of light energy. However, due to presence of positive charge and different functional groups chitosan possesses various chemical reactions such as hydrogen bonding, electrostatic interaction and π-π stacking interactions which facilitates active binding of CS/ZnO NC with RB-5 dye molecules in dark (Sakar et al., 2018). In the current study the RB-5 degradation rate under dark conditions is almost 80 % at dye concentration of 25 mg/mL which is similar to studies conducted by Chaisorn et al. (Chaisorn et al., 2023).

For phytotoxicity evaluation of ZnO NPs and CS/ZnO NC on wheat plants, various concentrations (0.25, 0.5,1 and 2 mg/mL) of catalysts were applied to wheat plants. The concentration dependent improvements in growth parameters were observed in wheat plant up to 1 mg/mL and decline in growth of wheat plant was observed at high concentration (2 mg/mL). This implies that ZnO NPs did not cause phytotoxic effects in wheat plants up to 1 mg/mL which might be due to increase in chlorophyll and photosynthetic rate and regulation of auxins and cytokines levels (Hamzah et al., 2022). Additionally, Zn cope with many environmental stresses to plant by properly activation antioxidant enzymes such as POD, CAT and SOD which help in neutralizing reactive oxygen species (ROS) and protect wheat cells from oxidative damage (Hasanuzzaman et al., 2020). These findings are very similar to those conducted by Khan et al. (2023) reporting that ZnO NPs could enhance the biomass, SL, RL and antioxidant levels as compared to control at low concentration. Better efficiency of CS/ZnO NC than ZnO NPs is due to Zn encapsulation into CS matrix, which regulate Zn release in adequate amount when require (Al-Nemrawi et al., 2022). Similar study also

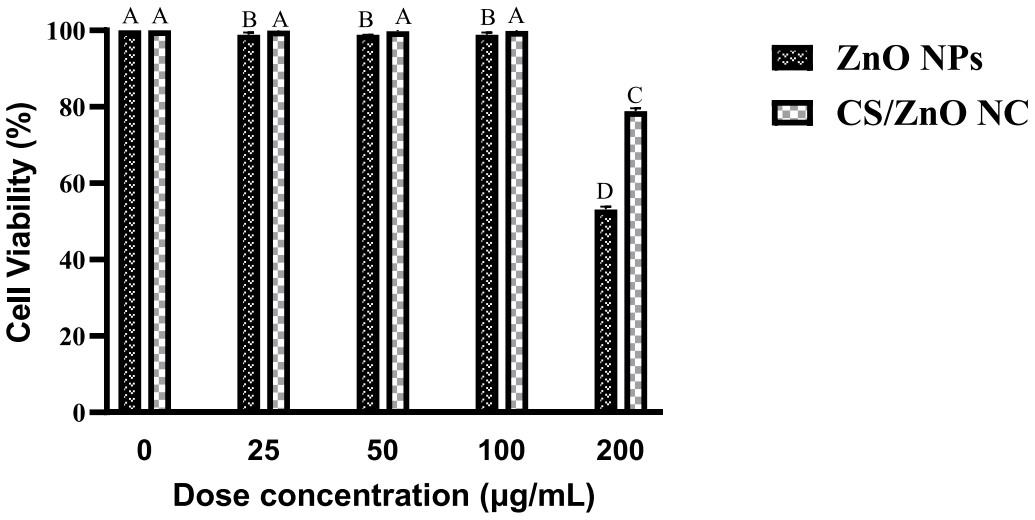

Fig. 8. In vitro viability of RPE normal cell line incubated after treatment with different concentrations of ZnO NPs and CS/ZnO NC.

reported by (Bashal et al., 2022) explains Zn mechanism in reducing ROS molecules with negatively effect on free radicles such as Superoxides (O^{2-}), hydroxyl radicals (OH^{-}) and hydrogen peroxide (H_2O_2) (Huang et al., 2019).

The study also assessed the cytotoxicity of ZnO NPs and CS/ZnO NC on the RPE human cell line, finding no significant impact on cell viability. While low concentrations of Zn^{2+} ions are crucial for various cellular functions and metabolism, elevated levels can induce apoptosis. Additionally, the results suggest that CS/ZnO NC could serve as advanced nano-fertilizers, enhancing wheat growth by providing essential nutrients through Zn encapsulation in the chitosan matrix without interfering with other mineral deposits.

5. Conclusion

In summary, CS/ZnO nanocomposites were synthesized using microbial methods with chitosan as a stabilizer. The nanocomposites showed a significant increase in dye adsorption, achieving up to 95 % degradation of the dye due to the enhanced surface area of the polymer. A concentration of 1 mg/mL of ZnO nanoparticles or chitosan/ZnO nanocomposites was safe for plant application, and 100 µg/mL of these materials had no cytotoxic effects on human cell lines.

Ethical approval

The authors declare that they followed all the rules mentioned in the "instruction for authors." This manuscript was not submitted to any journal. This submitted work is original and all the results are concluded honestly.

Funding

Financial support provided by Researchers Supporting Project, number (RSPD2024R637), King Saud University, Riyadh, Saudi Arabia to complete this research. A partial funding from the annual departmental research budget of Department of Bioinformatics and Biotechnology, Government College University Faisalabad, Pakistan is also acknowledged.

CRediT authorship contribution statement

Syeda Khola Tazeen: Formal analysis, Investigation, Methodology, Writing – original draft. **Muhammad Bilal Khan Niazi:** Writing – review & editing, Funding acquisition, Conceptualization. **Manal Abdulaziz Binobead:** Funding acquisition, Writing – review & editing. **Temoor Ahmed:** Investigation, Writing – review & editing. **Muhammad Shahid:** Writing – review & editing, Funding acquisition, Conceptualization.

Declaration of competing interest

The authors declare that they have no known competing financial interests or personal relationships that could have appeared to influence the work reported in this paper.

Data availability

The data that support the findings of this research are available on request from the corresponding author.

Acknowledgements

The authors are thankful to the all the co-authors. Authors also acknowledge research support of Dr. Qasim Ali (Assistant Professor) from Department of Botany, Government Colledge University Faisalabad in the form of chemical and reagents to perform Plant pytotoxicity experiment. The authors extend their appreciations to Dr. Muhammad Zubair (Assistant professor) from Department of Biotechnology, Government Colledge University Faisalabad for cooprating in cytotocity evaluation.

Appendix A. Supplementary data

Supplementary data to this article can be found online at https://doi.org/10.1016/j.jksus.2024.103432.

References

Adeel, M., Saeed, M., Khan, I., et al., 2021. Synthesis and characterization of Co-ZnO and evaluation of its photocatalytic activity for photodegradation of methyl orange. ACS Omega 6 (2), 1426–1435. https://doi.org/10.1021/acsomega.0c05092.

Ali, S., Dayo, M., Alahmadi, S., et al., 2024. Chitosan-supported ZnO nanoparticles: their green synthesis, characterization, and application for the removal of pyridoxine HCl (Vitamin B6) from aqueous media. Molecules 29 (4), 828.

Al-Nemrawi, N.K., Alkhatib, R.Q., Ayyad, H., et al., 2022. Formulation and characterization of tobramycin-chitosan nanoparticles coated with zinc oxide nanoparticles. Saudi Pharm. J. 30 (4), 454–461. https://doi.org/10.1016/j.jsps.2022.01.016.

Alzahrani, E.A., Nabi, A., Kamli, M.R., et al., 2023. Facile green synthesis of ZnO NPs and plasmonic Ag-supported ZnO nanocomposite for photocatalytic degradation of methylene blue. Water 15 (3), 384.

Bashal, A.H., Riyadh, S.M., Alharbi, W., et al., 2022. Bio-based (Chitosan-ZnO) nanocomposite: synthesis, characterization, and its use as recyclable, ecofriendly biocatalyst for synthesis of thiazoles tethered azo groups. Polymers 14 (3), 386. https://doi.org/10.3390/polym14030386.

Batra, V., Kaur, I., Pathania, D., et al., 2022. Efficient dye degradation strategies using green synthesized ZnO-based nanoplatforms: a review. Appl. Surf. Sci. Adv. 11, 100314 https://doi.org/10.1016/j.apsadv.2022.100314.

Ben Amor, I., Hemmami, H., Laouini, S.E., et al., 2022. Sol-Gel synthesis of ZnO nanoparticles using different chitosan sources: effects on antibacterial activity and photocatalytic degradation of AZO dye. Catalysts 12 (12), 1611.

Bui, V.K.H., Park, D., Lee, Y.-C., 2017. Chitosan combined with ZnO, TiO_2 and Ag nanoparticles for antimicrobial wound healing applications: a mini review of the research trends. Polymers 9 (1), 21.

Castillo-Suarez, L.A., Sierra-Sanchez, A.G., Linares-Hernandez, I., et al., 2023. A critical review of textile industry wastewater: green technologies for the removal of indigo dyes. Int. J. Environ. Sci. Technol.: IJEST 1–38. https://doi.org/10.1007/s13762-023-04810-2.

Chaisorn, W., Nuengmatcha, P., Noypha, A., et al., 2023. Adsorption-photocatalytic degradation abilities of gamma-irradiated chitosan-ZnO-AgNP composite for organic dye removal and antibacterial activity. Environ. Sci. Pollut. Res. Int. 30 (43), 96840–96859. https://doi.org/10.1007/s11356-023-29305-y.

Díaz, C., Segovia, M., Valenzuela, M.L., 2022. Solid state nanostructured metal oxides as photocatalysts and their application in pollutant degradation: a review. Photochem. 2 (3), 609–627. https://doi.org/10.3390/photochem2030041.

González-Fragozo, H. E., Zabaleta-Solano, C., Devia-González, J., et al., 2020. Efecto del riego con agua residual tratada sobre la calidad microbiológica del suelo y pasto King Grass. Revista U.D.C.A Actualidad & Divulgación Científica. 23 (2) doi: 10.31910/rudca.v23.n2.2020.1513.

Hamzah, S.M., Usman, K., Rizwan, M., et al., 2022. Functions and strategies for enhancing zinc availability in plants for sustainable agriculture. Front. Plant Sci. 13, 1033092. https://doi.org/10.3389/fpls.2022.1033092.

Hasanuzzaman, M., Bhuyan, M., Zulfiqar, F., et al., 2020. Reactive oxygen species and antioxidant defense in plants under abiotic stress: revisiting the crucial role of a universal defense regulator. Antioxidants 9 (8). https://doi.org/10.3390/antiox9080681.

Hassaan, M., El Katory, M., Ali, R., et al., 2019. Photocatalytic degradation of reactive black 5 using Photo-Fenton and ZnO nanoparticles under UV irradiation. Egypt. J. Chem. https://doi.org/10.21608/ejchem.2019.15799.1955.

Huang, H., Ullah, F., Zhou, D.X., et al., 2019. Mechanisms of ROS regulation of plant development and stress responses. Front. Plant Sci. 10, 800. https://doi.org/10.3389/fpls.2019.00800.

Jyoti, S., Singh, S.D., et al., 2023. Comparative study for removal of toxic hexavalent chromium by zinc oxide nanoparticles, chitosan, chitin and zinc-chitosan nano-biocomposite. Environ. Technol. Innov. 32, 103310 https://doi.org/10.1016/j.eti.2023.103310.

Khan, S., Al-Qurainy, F., Al-Hashimi, A., et al., 2023. Effect of green synthesized ZnO-NPs on growth, antioxidant system response and bioactive compound accumulation in Echinops macrochaetus, a potential medicinal plant, and assessment of genome size (2C DNA Content). Plants 12 (8), 1669. https://doi.org/10.3390/plants12081669.

Kumar, S., Koh, J., 2012. Physiochemical, optical and biological activity of chitosan-chromone derivative for biomedical applications. Int. J. Mol. Sci. 13 (5), 6102–6116. https://doi.org/10.3390/ijms13056102.

Kumar, S., Ye, F., Mazinani, B., et al., 2021. Chitosan nanocomposite coatings containing chemically resistant ZnO–SnOx core–shell nanoparticles for photocatalytic antifouling. Int. J. Mol. Sci. 22 (9), 4513. https://doi.org/10.3390/ijms22094513.

Maeda, K., 2011. Photocatalytic water splitting using semiconductor particles: history and recent developments. J. Photochem. Photobiol. C: Photochem. Rev. 12 (4), 237–268. https://doi.org/10.1016/j.jphotochemrev.2011.07.001.

Malagutti, A.R., Mourao, H.A., Garbin, J.R., et al., 2009. Deposition of TiO_2 and Ag: TiO_2 thin films by the polymeric precursor method and their application in the photodegradation of textile dyes. Appl. Catal. B 90 (1–2), 205–212.

Malekkiani, M., Heshmati Jannat Magham, A., Ravari, F., et al., 2022. Facile fabrication of ternary MWCNTs/ZnO/Chitosan nanocomposite for enhanced photocatalytic degradation of methylene blue and antibacterial activity. Sci. Rep. 12 (1), 5927. https://doi.org/10.1038/s41598-022-09571-5.

Maliki, S., Sharma, G., Kumar, A., et al., 2022. Chitosan as a tool for sustainable development: a mini review. Polymers 14 (7), 1475.

Maruthupandy, M., Muneeswaran, T., Anand, M., et al., 2020. Highly efficient multifunctional graphene/chitosan/magnetite nanocomposites for photocatalytic degradation of important dye molecules. Int. J. Biol. Macromol. 153, 736–746. https://doi.org/10.1016/j.ijbiomac.2020.03.045.

Mathiarasu, R.R., Manikandan, A., Panneerselvam, K., et al., 2021. Photocatalytic degradation of reactive anionic dyes RB5, RR198 and RY145 via rare earth element (REE) lanthanum substituted $CaTiO_3$ perovskite catalysts. J. Mater. Res. Technol. 15, 5936–5947. https://doi.org/10.1016/j.jmrt.2021.11.047.

Mekahlia, S., Douadi, T., 2021. Chitosan–ZnO nanocomposite from a circular economy perspective: in situ cotton-used fabric recycling and the nanocomposite recovering. Polym. Bull. 79 (9), 7491–7529. https://doi.org/10.1007/s00289-021-03859-8.

Mutukwa, D., Taziwa, R.T., Khotseng, L., 2022. Antibacterial and photodegradation of organic dyes using lamiaceae-mediated ZnO nanoparticles: a review. Nanomaterials (Basel) 12 (24). https://doi.org/10.3390/nano12244469.

Noman, M., Ahmed, T., Shahid, M., et al., 2021. Biogenic copper nanoparticles produced by using the *Klebsiella pneumoniae* strain NST2 curtailed salt stress effects in maize by modulating the cellular oxidative repair mechanisms. Ecotoxicol. Environ. Saf. 217, 112264 https://doi.org/10.1016/j.ecoenv.2021.112264.

Picos-Corrales, L.A., Morales-Burgos, A.M., Ruelas-Leyva, J.P., et al., 2023. Chitosan as an outstanding polysaccharide improving health-commodities of humans and environmental protection. Polymers 15 (3), 526.

Preethi, S., Abarna, K., Nithyasri, M., et al., 2020. Synthesis and characterization of chitosan/zinc oxide nanocomposite for antibacterial activity onto cotton fabrics and dye degradation applications. Int. J. Biol. Macromol. 164, 2779–2787. https://doi.org/10.1016/j.ijbiomac.2020.08.047.

Rahman, T.U., Roy, H., Shoronika, A.Z., et al., 2023. Sustainable toxic dye removal and degradation from wastewater using novel chitosan-modified TiO_2 and ZnO nanocomposites. J. Mol. Liq. 388, 122764 https://doi.org/10.1016/j.molliq.2023.122764.

Sabrin, A., Arafat, A., 2015. Textile dye removal from wastewater effluents using Chitosan-ZnO nanocomposite. J. Text. Sci. Eng. 5 (3) https://doi.org/10.4172/2165-8064.1000200.

Sakar, M., Nguyen, C.-C., Vu, M.-H., et al., 2018. Materials and mechanisms of photo-assisted chemical reactions under light and dark conditions: can day-night photocatalysis be achieved? ChemSusChem 11 (5), 809–820. https://doi.org/10.1002/cssc.201702238.

Samsami, S., Mohamadizaniani, M., Sarrafzadeh, M.-H., et al., 2020. Recent advances in the treatment of dye-containing wastewater from textile industries: overview and perspectives. Process Saf. Environ. Prot. 143, 138–163. https://doi.org/10.1016/j.psep.2020.05.034.

Shi, Y., Chang, Q., Zhang, T., et al., 2022. A review on selective dye adsorption by different mechanisms. J. Environ. Chem. Eng. 10 (6), 108639 https://doi.org/10.1016/j.jece.2022.108639.

Singh, K., Maurya, S., Gupta, S., et al., 2023. Effect of the standardized ZnO/ZnO-GO filter element substrate driven advanced oxidation process on textile industry effluent stream: detailed analysis of photocatalytic degradation kinetics. ACS Omega 8 (31), 28615–28627. https://doi.org/10.1021/acsomega.3c03122.

Thamilarasan, V., Sethuraman, V., Gopinath, K., et al., 2018. Single step fabrication of chitosan nanocrystals using penaeus semisulcatus: potential as new insecticides, antimicrobials and plant growth promoters. J. Clust. Sci. 29 (2), 375–384. https://doi.org/10.1007/s10876-018-1342-1.

Zaman, H.G., Baloo, L., Aziz, F., et al., 2022. COD adsorption and optimization from produced water using chitosan–ZnO nanocomposite. Appl. Nanosci. 12 (6), 1885–1898. https://doi.org/10.1007/s13204-022-02392-y.

Zeghoud, S., Hemmami, H., Ben Seghir, B., et al., 2022. A review on biogenic green synthesis of ZnO nanoparticles by plant biomass and their applications. Mater. Today Commun. 33, 104747 https://doi.org/10.1016/j.mtcomm.2022.104747.